# Template-Directed Materials for Rechargeable Lithium-Ion Batteries†

Fangyi Cheng, Zhanliang Tao, Jing Liang, and Jun Chen*

*Institute of New Energy Material Chemistry and Engineering Research Center of Energy Storage and Conversion (Ministry of Education), Nankai University, Tianjin 300071, P.R. China*

*Received July 30, 2007. Revised Manuscript Received November 9, 2007*

Extensive research activities have been directed to develop flexible rechargeable lithium-ion batteries with large capacity, high power, and long cycling life. Template technology offers the benefits in terms of either designing new-type electrode materials or modifying traditional battery configurations. With the aid of "hard" or "soft" templates, a variety of functional materials with diverse structures and morphologies such as one-dimensional (1D) nanostructures, 2D films, and 3D porous frameworks have been synthesized. This review highlights the recent progress in the template-prepared electrode materials for lithium storage, mainly focusing on the $Li^+$ intercalation reactions and the Li conversion properties with the nanostructures of $LiCoO_2$, C, $SnO_2$, $Fe_2O_3$, $Co_3O_4$, $VO_x$, and $MnO_2$. In some specifically demonstrated examples, the templated cathode materials (e.g., lithium metal oxides) show significantly improved reversibility and high rate capability over a voltage of 3 V after 100 cycles, whereas the templated anode materials (e.g., metal oxides) can deliver high capacity exceeding 1000 mA h $g^{-1}$. The structural and morphological merits of the template-directed materials have been especially addressed in comparison with their traditional bulk forms.

## Introduction

Lithium is the lightest metal (equivalent weight 6.94 g/mol and specific gravity 0.53 g/$cm^3$) in the elemental table and thus can deliver high energy density per electron. The theoretical electrochemical capacity of Li to $Li^+$ is 3860 mA h $g^{-1}$. The storage and transportation of solid-state lithium in an inert environment is much easier than that of gaseous hydrogen, rendering it a good energy carrier. In the 1970s, Li metal was first employed as negative electrode materials to assemble primary Li cells.[1] Later on, a series of intercalation compounds such as dichalcogenide (especially $TiS_2$) were developed and demonstrated to react reversibly with lithium, leading to the initiation of rechargeable Li-ion batteries.[2] These batteries, with the utilization of lithiated metal oxide and graphite, have dominated the rechargeable power source market ever since the first successful commercialization in the 1990s.[3] Compared with traditional secondary cells such as lead-acid or nickel-cadmium batteries, rechargeable lithium-ion batteries exhibit superior performance including long cycle life, high specific energy, and no memory effect.[3] Because of these advantages, they cover a wide variety of applications ranging from consumer electronics (e.g., laptop computers, cell phones, and cameras) to electric vehicles (e.g., hybrid electric cars and all-electric scooters).[1–4] Nowadays, Li-ion cells are constructed with various shapes (cylindrical, coin, or prismatic shape) by employing different electrode materials.

Rechargeable batteries are the representative system for the storage and conversion of electrochemical energy. Following a fundamental conversion equation $\Delta G = -nFE$ ($\Delta G$ is the change in Gibbs free energy, $n$ is the electron transfer number, $F$ is Faraday constant, and $E$ is the cell potential), a rechargeable battery is one or several electrically connected cells for generating electricity when discharged and storing chemical energy after being charged. Each cell consists of a positive (cathode) and a negative (anode) electrode, together with an electrolyte-filled separator that allows ion transfer but prohibits electrical contact. For a lithium-ion battery, the anode is usually composed of lithium metal or lithium insertion/conversion compound, whereas the cathode is made up of another $Li^+$ host material possessing a much more positive redox potential.[5] As shown in Figure 1, the basic operating principle is based on $Li^+$ intercalation/conversion reactions. When the cell is discharged, $Li^+$ intercalates the positive materials through the electrolyte, providing outer electron flow. On charge, $Li^+$ deintercalates in reverse from the cathode and intercalates/enters the anode. Li-ion shuttles between the cathode and the anode during

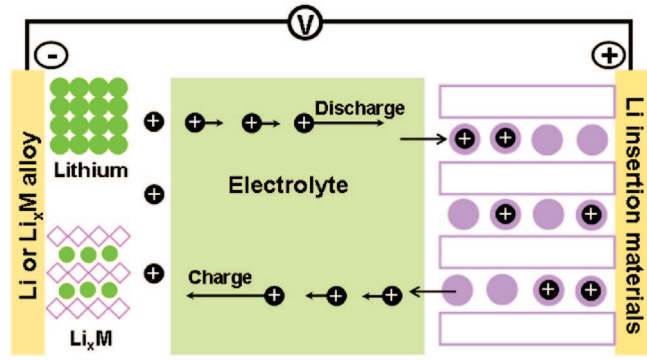


**Figure 1.** Schematic operating principle of traditional rechargeable lithium-ion batteries.

† Part of the "Templated Materials Special Issue".

* Corresponding author. E-mail: chenabc@nankai.edu.cn.

10.1021/cm702091q CCC: $40.75 
Published on Web 12/28/2007

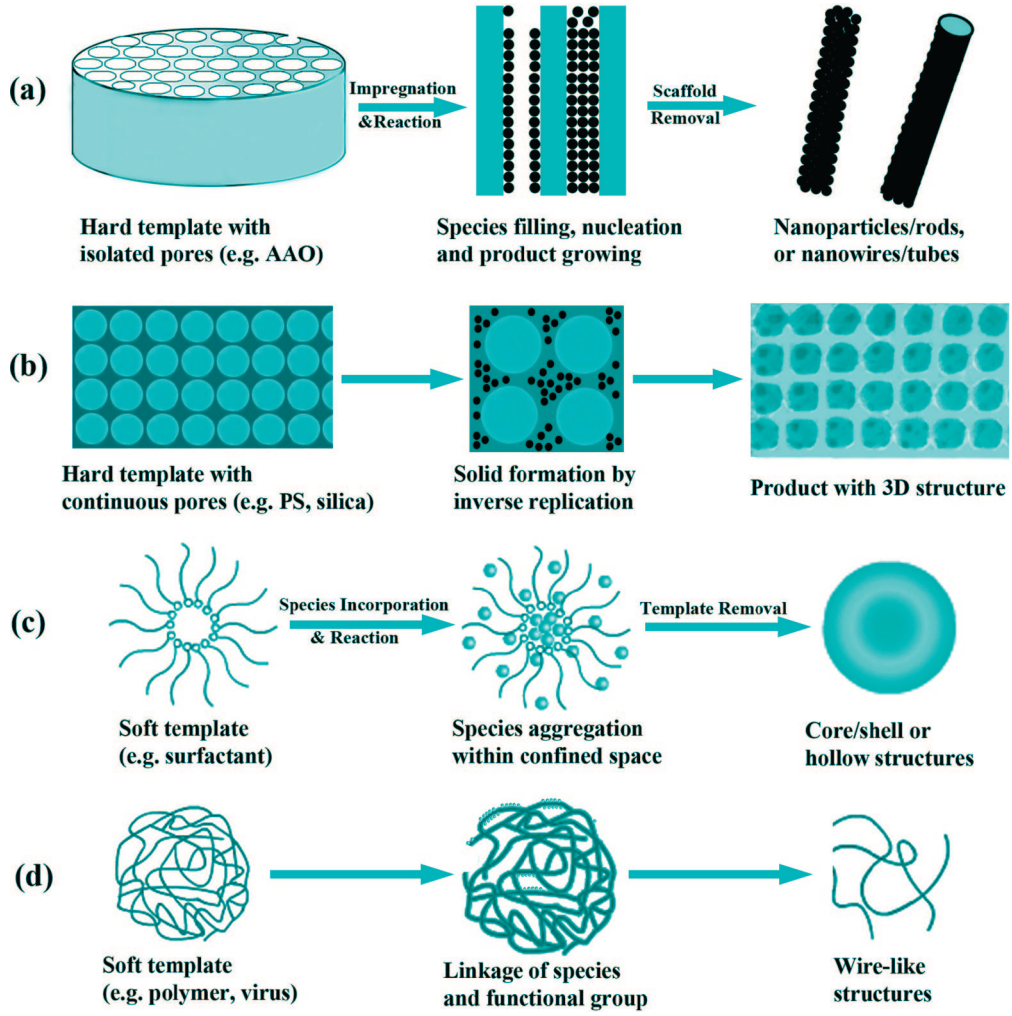


**Figure 2.** Schematic depiction showing some typical examples of the hard and soft template synthesis of electrode materials with diverse morphologies.

the cycling process, enabling the conversion and storage of electrochemical energy within the cells. Therefore, the performance of rechargeable Li-ion batteries strongly depends on the active materials employed for Li storage. To attain high specific capacity, electrode materials should reversibly accommodate a large amount of lithium while fast ionic/electronic transfer in the cell is required to achieve high current density (namely, power capability).

In commercial Li-ion batteries, carbons and lithium metal oxides are commonly employed as the negative and positive electrode materials, respectively. The chemical reactions involved in the cell can be briefly described as

$$\textbf{Negative:}\ C + xLi^+ + xe^- \underset{\text{discharge}}{\overset{\text{charge}}{\rightleftharpoons}} LixC$$

$$\textbf{Positive:}\ LiMO_2 \underset{\text{discharge}}{\overset{\text{charge}}{\rightleftharpoons}} Li_{1-x}MO_2 + xLi^+ + xe^-$$

$$\textbf{Overall:}\ LiMO_2 + C \underset{\text{discharge}}{\overset{\text{charge}}{\rightleftharpoons}} Li_xC + Li_{1-x}MO_2$$

For typical carbon materials such as graphite, the basic building unit is a planar sheet of carbon atoms arranged in a hexagonal array. Lithium intercalates into the carbon layer to form $Li_xC$ alloy, delivering a theoretical specific capacity of 372 mA h $g^{-1}$ ($LiC_6$) and a potential plateau lower than 0.5 V vs $Li^+/Li$.[6] The practical performance of carbonaceous materials strongly depends on their crystallinity, microstructure and morphology.[6,7] As typical positive electrode materials, lithiated transition metal oxide such as $LiCoO_2$ possesses 2D layered crystal structure (see Figure 3 infra) and exhibits high voltage approaching 4 V vs Li and can thus offer a high specific energy of 1017 W h $kg^{-1}$.[5] Therefore, lithium-ion batteries based on $LiCoO_2$ and graphite electrodes outperforms other types of rechargeable cells such as lead-acid and nickel-based systems especially in regard to energy density.[2] However, further advancements in current lithium-ion batteries are still somewhat bottlenecked by limitation in electrode materials associated with limited capacity, lack of shape flexibility, or safety problems.

The improvement searched in active materials mainly concerns high reversible capacity, structural flexibility and stability, fast $Li^+$ diffusion at a high rate, low cost, and being environmentally benign.[3] Extensive efforts have been dedicated to fulfilling these goals by either designing new types of active materials or modifying traditional electrodes. For example, aiming for cheap yet high energy lithium-ion batteries with various transition metal oxides and Sn-based anode materials were explored, demonstrating significantly larger specific capacity than that obtained by commercial graphite.[8,9] The intensively studied cathode materials mainly include nickel/manganese-based lithium metal oxides[1,5] and olivine phases, in particu-

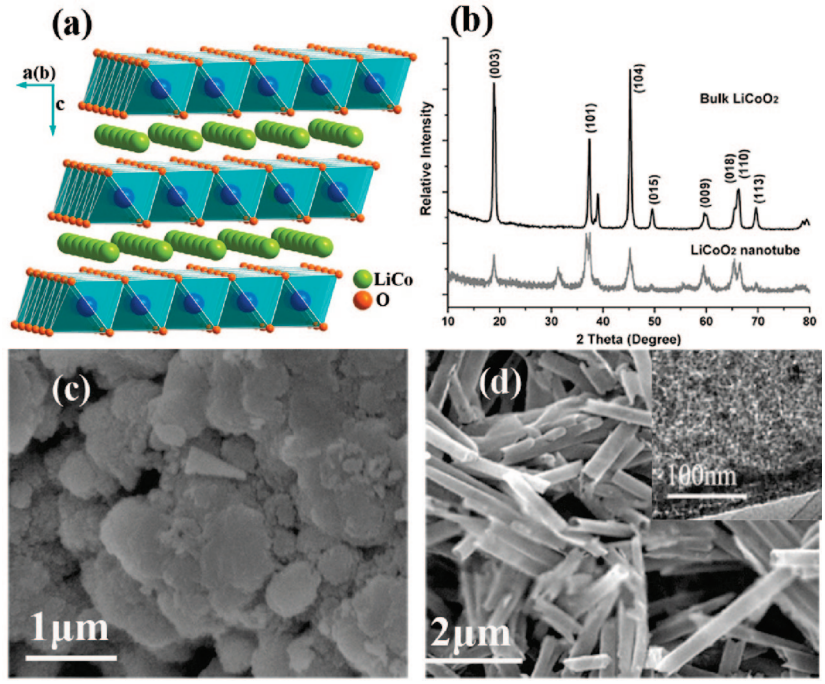


**Figure 3.** (a) Crystal structure of $LiCoO_2$. (b) XRD patterns and SEM micrographs of (c) bulk $LiCoO_2$ and (d) the template-prepared $LiCoO_2$ nanotubes. The inset of (d) shows the TEM image of one part of a single nanotube composed of binding nanoparticles.

lar, lithium iron phosphate ($LiFeO_4$).[10,11] Having obtained the high stability and conductivity, these active materials would have a major impact in electrochemical energy storage and find promising applications in the next-generation rechargeable batteries.

Meanwhile, nanostructures of traditional electrode materials, because of their novel properties associated with decreased size, unique shape, and defective nature, have been widely studied and demonstrated to exhibit superior characteristics to the bulk counterparts.[12–14] The template technique is versatile to construct advanced materials with controlled structures and desired functions.[15–18] Template-directed materials generally possess structural and morphological abundance due to the diversity of employed template precursors. Nano/microscaled electrode materials with different morphologies such as one-dimensional (1D) wire/tube structures, 2D films, and 3D interconnected porous architectures can be obtained through the template synthesis method. The template-synthesized materials normally exhibit small crystalline size, high surface area, large surface-to-volume ratio, and favorable structural stability. These characteristics are beneficial to the electrochemical properties because they would lead to fast ion/electron transfer, sufficient contact between active materials and electrolyte, and enhanced flexibility. Improved electrode performances such as higher overall capacity, better high-rate capability, and longer cycling life can be expected accordingly. Therefore, introducing template technique in preparing and assembling electrode materials may offer new opportunities to further increase the performance of the existing lithium battery system.

Pioneering work carried out by Martin and co-workers has shown that template synthesis is a useful method to generate nanomaterials for diverse potential applications.[19] An early short review on the membrane template-prepared materials for Li-ion batteries was presented by the same group in 2002.[20] Ever since then, much more progress has been made in both the template synthesis and the applications of templated materials for lithium storage. On one hand, a variety of materials ranging from inorganic/organic compounds to polymers and even biological materials have been employed as templates without limitation to membranes. On the other hand, various electrode materials with diverse compositions, structures, and morphologies have been obtained through the template synthesis route. In this article, we review the recent progress made in the template-directed materials for rechargeable lithium-ion batteries. The discussion of the detailed synthesis method is not the main concern in the scope of this article because the template synthesis is a common topic and has been well-reviewed elsewhere.[15–18] Instead, some overall concept of template synthesis will be mentioned. We intend to focus on the most widely investigated templated negative and positive electrode materials, mainly including lithiated transition metal oxide, carbon, and metal oxide. Furthermore, we wish to address the structural and morphological advantages of the template-directed materials for lithium storage.

## Template Synthesis

Generally, the employed materials in template synthesis can be simply classified into hard templates and soft templates. The so-called "hard templates" normally possess well-confined void, which is in the form of channels, pores, or connected hollow space. Anodic aluminum oxide (AAO) membranes and silica are typical examples of this type. The so-called "soft templates" usually consist of organic surfactants, polymers, and even biological viruses, which are relatively flexible in shape. Clear definition of "hard" or

"soft" is not easy in some cases such as porous polymer membranes, which possess confined inner hollow space nevertheless exhibit somewhat structural flexibility. Figure 2 illustrates the representative concept of the template synthesis. The overall process generally involves the following procedures: (1) precursors combine with templates by impregnation or incorporation; (2) solid species form through reaction, nucleation and growth; and (3) product is obtained after template removal. Templates can be employed to various synthetic techniques such as sol–gel synthesis, chemical vapor deposition, thermal decomposition, electrodeposition, solvothermal preparation, and so on.

For hard templates, the connectivity of the pores or channels strongly influences the structure of the resulting solid product. In the case of nonconnected porous templates such as AAO membranes and MCM-41 silica, solid product forms inside the isolated pores, replicating the shape of the void space in templates.[18] As a result, aligned structures such as 1D nanotubes and nanowires are usually obtained after removing the template scaffold (Figure 2a). The templates that consist of a continuous pore system such as porous carbons or silica gels generally lead to an inverse replica of the mold structure after template isolation, thus resulting in frameworks with interconnected 3D pores (Figure 2b).[21] The most widely used hard templates are AAO membranes because of their facile preparation and controllable pore size.[22] In our group, by applying AAO template synthesis, we have obtained a series of inorganic electrode materials including metals,[23] metal oxides[24] and hydroxides,[25] lithium metal oxide,[26] and composite metal oxide.[27]

For soft templates, they function as structure-directing agents that assist in the assembly of reacting species. Soft templates are facile for controlled fabrication of nanomaterials because of either the unique anisotropic structures or the functionality of their subunit groups. Typical examples are surfactants, long-chain polymers, and viruses. Under a certain condition, these materials are assembled into the form of aggregating entities such as micelle/vesicle aggregates or liquid crystal phase, which restrict and direct the growth of a guest structures.[28] Precursor species react in the confined space of surfactant micelles (Figure 2c) or on the surface of polymer/virus chains (Figure 2d), as driven by self-assembly or interaction between functional groups.[29,30] After separating the template, spherelike or wirelike structures can be fabricated, following the basic shape of the aggregates. In many cases, porous nanostructures are obtained during such a "nanocasting" process.[31] The main strategy of this synthesis route is based on the transcriptive and/or synergistic effect of the soft templates.

Various lithium storage materials such as lithiated metal oxides (e.g., $LiCoO_2$ and $LiMn_2O_4$), carbons, tin-based oxides, and transition metal oxides (e.g., $Fe_2O_3$, $Co_3O_4$, NiO, $VO_x$, $TiO_2$, $MnO_2$, etc.) can be obtained through the template synthesis route, as demonstrated in the following sections. Meanwhile, the template-prepared electrode materials usually possess controlled nanostructures with different size, shape, and dimension. For example, 1D nano/microarrays, 2D films, and 3D interconnected and ordered porous structures have been obtained by using different types of templates. The related novel structures and morphologies of these templated materials may facilitate the $Li^+$ intercalation and lithium transition reactions, and electrochemical properties that are superior to those of their bulk counterparts can be expected.

## Lithium Metal Oxide

The current commercial success of rechargeable lithium-ion batteries to a large extent relies on the employment of lithium metal oxides as the positive active materials. Lithium metal oxides generally possess layered or tunneled structures for reversible intercalation and deintercalation of lithium ions. These materials are typically stable to air and moisture, and commonly exhibit potential region higher than 3 V with flat plateau to host lithium. Among the family of lithium transition metal oxides, $LiCoO_2$, $LiNiO_2$, $LiMn_2O_4$, and their doped structures are most extensively investigated. In this section, we mainly focus on the recent report of the template synthesis and lithium-storage application of these cathode materials, together with a brief discussion of $Li_4Ti_5O_{12}$.

**Lithium Cobalt (nickel) Oxide.** $LiCoO_2$ and $LiNiO_2$ possess 2D crystal structure of the $\alpha$-$NaFeO_2$ type with the oxygen atoms in a cubic close-packed (ccp) arrangement (see Figure 3a). On complete delithiation of $LiCoO_2$, the oxygen layers rearrange into hexagonal close packing of the oxygen in the form of $CoO_2$. Several phases exist between the composition limits of $LiCoO_2$ and $CoO_2$, with varying degrees of distortion of the ccp oxygen lattice.[32] $LiCoO_2$ can deliver a high voltage plateau when charged and discharged (theoretical specific capacity is 274 mA h $g^{-1}$ if considering complete removal of lithium). However, reversible cycling can be carried out only in a limited range of composition. This limitation is related to the variation of crystal structure and the corrosion problem caused by the high oxidizing capability of the almost delithiated $Li_xCoO_2$ (when $x < 0.3$). The comparative isostructural $LiNiO_2$ is attractive because of its economic advantage and relatively lowered redox potential.[5] Unfortunately, stoichiometric $LiNiO_2$ is difficult to prepare and suffers from unstable problems. Cobalt-doped $LiNiO_2$, such as $LiNi_{0.5}Co_{0.5}O_2$, is much easier to obtain and offers a more negative potential while maintain structural stability. Therefore, further improving the practical capacity of $LiCoO_2$ and optimizing procedures for the preparation of Codoped $LiNiO_2$ are of great importance, because the capacities of current rechargeable batteries are usually cathode limited. Template-prepared $LiCoO_2$ and $LiNi_{0.5}Co_{0.5}O_2$ have been demonstrated to show much improved electrode performance than that of their bulk form and even outperform the nanoparticles counterparts obtained without template.[26,33–39]

$LiCoO_2$ and $LiNi_{0.5}Co_{0.5}O_2$ naontubes were prepared through the thermal decomposition of sol–gel precursors within the pores of AAO membranes.[26] As shown in Figure 3b, the templated nanotubes display similar XRD pattern to that of bulk $LiCoO_2$. However, the main diffraction peaks of the nanotubes are somewhat broadened and the relative peak intensity are much lower in comparison with that of the bulk forms. This difference can be ascribed to the polycrystalline character and the small particle size of the tubes. SEM micrographs reveal that the bulk $LiCoO_2$ materials are composed of irregular agglomerate particles

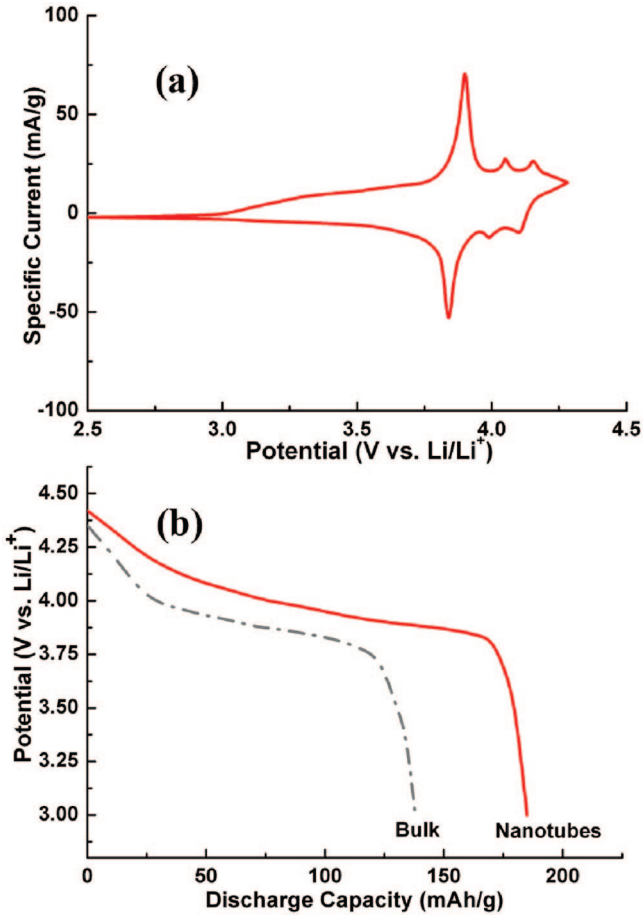


**Figure 4.** Cyclic voltammogramms (a) and discharge curves (b) of the templated $LiCoO_2$ nanotubes and bulk $LiCoO_2$ Adapted with permission from ref 26. Copyright 2005 American Chemical Society.

with micrometer size (Figure 3c), whereas the templated samples are present in straight tubular structure with open ends and relatively uniform diameters (Figure 3d). The walls of the tubes consist of binding nanocrystals, as shown in the enlarged TEM image (inset of Figure 3d). The present AAO template synthesis method, in combination with the thermal decomposition of sol–gel, is applicable to other 1D nanostructures especially nanotubes of $LiMn_2O_4$, $LiNi_{1-x}Co_xO_2$, and other doped lithium transition-metal oxides.

The template-directed $LiCoO_2$ nanotubes exhibit well-defined cathodic and anodic current peaks in the cyclic voltammogramms (CVs, Figure 4a).[26] The presented three sets of peaks are indicative of the lithium intercalation process (the first set) and the order–disorder phase transition (the second and third sets). In the case of bulk $LiCoO_2$, CVs of similar shape were observed except for lower peak current density and slightly enlarged potential separation between anodic and cathodic peaks (data not shown here). The discharge curve of $LiCoO_2$ nanotubes displays a relatively flatter and longer voltage plateau than that of the bulk counterparts (Figure 4b). This improvement is apparently derived from the advantageous properties of the templated 1D nanostructures as both the bulk and tubular $LiCoO_2$ were prepared under the same reaction conditions. The nanosize open-ended tubular structure could provide extra space and paths for electrolyte penetration and diffusion and thus enhance the contact between the electrolyte and the active materials. Additionally, the transfer length of electrons and ions may be shortened because of the small particle size of the binding nanocrystals that make up the tube walls. Therefore, the templated tubular morphology facilitates the efficient utilization of $LiCoO_2$. In our experiment, the nanotubes retained a considerably high capacity exceeding 150 mA h $g^{-1}$ after 100 cycles at constant charge/discharge current of 10 mA $g^{-1}$. Moreover, XRD and SEM analysis of the nanotube electrode taken after several electrochemical cycling showed that the crystal structure and 1D morphology were essentially preserved, with only a small change in cell parameters and partial tube aggregation.

Recently, Bruce and his collaborators reported the synthesis of nanowires and mesoporous low-temperature $LiCoO_2$ by a post-templating reaction.[34] The synthesis involves the procedures of a first preparation of mesoporous $Co_3O_4$ or nanowires followed by reaction of $Co_3O_4$ with LiOH after template removal, avoiding the direct reaction of the lithium precursor and the silica template. By using the hard template of SBA-15 and KIT-6, nanowires and mesoporous $LiCoO_2$ were respectively obtained, maintaining the nanostructured morphology of $Co_3O_4$. Preliminary electrochemical data indicated that the templated $LiCoO_2$ nanostructures exhibited remarkedly less fade in discharge capacity on cycling as compared to normal low-temperature $LiCoO_2$. Other forms of templated 1D lithium cobalt oxide nanostructures such as nanorods and nanowires arrays were also prepared and demonstrated to exhibit favorable electrochemical performance.[33]

Template synthesis is also useful to obtain 2D films of pure $LiCoO_2$ and partially substituted $LiCoO_2$ with improved electrode performance. For example, $LiCoO_2$ film was recently synthesized through sol–gel method using cellulose acetate membrane as the template.[35] This new film delivered approximately 2.5 times higher capacity than conventional $LiCoO_2$ film obtained by spin coating without template. CV and electrochemical impedance spectrum (EIS) results showed that better electrochemical stability and impedance behavior were achieved on the template-synthesized film electrode. The impedance of this film was 1 order of magnitude lower than that of conventional film, together with a significant decrease in charge-transfer resistance. These improved properties were attributed to the higher porosity of the templated films that reduced the interface resistance between the electrode and the electrolyte.[35] $LiNi_{1-x}Co_xO_2$ porous films were also prepared by combining a sol–gel method and a template approach.[36] These templated films resulted in marked intensification/definition of the redox reaction during lithium intercalation/deintercalation as well as a monotonous charge/discharge profile with a specific capacity of 130 mA h $g^{-1}$ and 100% Coulombic efficiency.

In addition to 1D and 2D morphology, $LiCoO_2$ nanoparticles were prepared by a sol–gel method assisted with triblock copolymer surfactant soft template, which exhibited high initial capacity and good cycling stability.[37] The template-directed $LiCoO_2$ nanoparticles could be further employed to prepare ultrathin-film electrode using computer jet-printing method, thus indicating their potential application

in thin-film lithium batteries. In another example, layered $LiNi_{0.5}Co_{0.5}O_2$ particles with sphere shape were synthesized by microwave-assisted method using polyacrylamide as the template.[38] The obtained particles retained a large discharge capacity of 145 mA h $g^{-1}$ after 20 cycles at a 0.2 C rate (the discharge of the full capacity in 5 h).

**Lithium Manganese (titanium) Oxide.** $LiMn_2O_4$ and $Li_4Ti_5O_{12}$ possess 3D crystal structure of spinel type. However, it should be noted that $LiMn_2O_4$ is a typical cathode material with 4 V potential range, whereas $Li_4Ti_5O_{12}$ is an attractive anode material because of its low $Li^+$ intercalation potential and relatively large capacity. $LiMn_2O_4$ nanoparticles, which were synthesized using ionically conducting block copolymer template, exhibited no appreciable capacity fade after 300 cycles.[40] The alumina template prepared $LiMn_2O_4$ nanotubes displayed flat discharge profile with a very nearly constant voltage during 95% of the full discharge process.[26] Zr and Co codoped $LiMn_2O_4$ nanowires were also fabricated using sol–gel−AAO template process and were expected to find promising application as cathode materials.[41]

Using colloidal templating process combined with the sol–gel method, Kanamura et al. synthesized 3D ordered macroporous membrane of Li−La−Ti−O (LLT) as well as the composite electrodes of LLT−$Li_4Ti_5O_{12}$ and LLT−$LiMn_2O_4$.[42] The obtained LLT showed a $Li^+$ conductivity of $10^{-3}$ S/m at room temperature, thus might find some potential application in all solid-state rechargeable lithium batteries. Poeppelmeier's group recently reported the synthesis of 3D ordered $Li_4Ti_5O_{12}$ macroporous structures and the study of their electrochemical properties.[43] The porous $Li_4Ti_5O_{12}$ with different filling fractions were prepared via a single step of metal−organic precursor method using non-cross-linked poly(methyl methacrylate) and polystyrene spheres as the template. These templated 3D structures demonstrated excellent rate capacity and extremely high reversible capacity. The enhanced performance was ascribed to the following morphological benefits. (1) The macroporous structure allows easier electrolyte penetration to every part of the particle. (2) The roughened and porous walls with increased surface-to-bulk ratio possess more sites for lithium ions to enter and allow facile lithium diffusion at higher current density. (3) Low-angle grain boundaries found in the wall help to expedite electrical conductivity and thus decrease polarization within the electrode. Therefore, all these examples demonstrated that templated nanostructures of traditional Li intercalation materials outperformed their bulk counterparts in improved capacity and enhanced rate and cycling performance.

## Carbon-Based Materials

Carbonaceous materials are currently predominant anode active materials in commercial rechargeable lithium-ion batteries. Carbon electrode materials can be generally divided into three structural classes including graphitic, soft (graphitizable), and hard (nongraphitizable) carbons. Electrochemical properties may vary because of their differences in crystalline structure, morphology, texture, and chemical composition.[44,45] Among various types of carbonaceous materials, graphitic carbon generally exhibits good reversibility, whereas the theoretical capacity is limited; nongraphite carbon can be highly lithiated but nevertheless lacks cycling capability. Therefore, extensive effort has been generated to develop new carbonaceous materials with both high and reversible capacity. The most extensively investigated template-directed carbons possess 1D nanostructure or porous structure.

**1D Nanostructured Carbons.** The application of nanostructured carbons, especially carbon nanotubes and nanowires, has received extensive interest.[46,47] Martin and coworkers reported the template preparation of carbon nanotubule membranes for electrochemical energy storage.[48] They prepared free-standing nanoporous carbon membranes and carbon nanotubules by chemical vapor deposition method combined with AAO template. According to their cyclic voltammograms (CV) results, the template-synthesized tubule membranes delivered a high $Li^+$ intercalation capacity of 490 mA h $g^{-1}$, whereas the capacity of the tube-in-tube carbon membrane was at least two times higher. Apparently, such unprecedented electrochemical activities of graphite carbon were ascribed to the templated nanotubular structure because the capacity of graphite carbon is generally lower than 400 mA h $g^{-1}$. Additionally, template-directed 1D nanocarbons showed high-rate capability due to their morphological benefits.[49] Another example of 1D nanostructure is carbon nanofilaments (CNFs), which were prepared by liquid phase carbonization using AAO membrane templates.[50] CNFs formed at elevated carbonization temperatures exhibited inferior reversible capacity, indicating that the presence of loops at the edge of graphene layers impedes the deep intercalation of Li ions. For 1D nanostructure, the diameter is an important parameter that influences their properties. For instance, narrower CNFs showed improved rate capability but increased irreversible initial capacity.[50] This observation can be interpreted by the decreased ionic diffusion length as well as easier platelet exfoliation and the formation of SEI film related to a reduced diameter. It should also be noted that decreased size might induce particle aggregation, which would counteract the beneficial effect of small diameter. Therefore, optimizing the size of 1D nanostructure is interesting and important.

**Porous Carbonaceous Materials.** Recently, template-prepared porous carbon materials have attracted much attention as promising materials for lithium storage. Ordered porous carbonaceous materials with different pore size ranging from subnanometer to micrometer scale have been prepared and electrochemically investigated. These templated porous carbons were usually demonstrated to show a prominently increased capacity in comparison with traditional graphitic carbons, although in many cases the irreversibility was also accompanied.

High-surface-area microporous carbon materials were synthesized and electrochemically analyzed by Takeuchi and co-workers.[51] Various inorganic materials such as zeolite (Y, Beta, ZSM-5) and montmorillonite clay (K10) were used as the template matrix to encapsulate organic precursors, which were polymerized and carbonized to form microporous carbons. The as-prepared carbons displayed high irreversible

capacities and significant voltage hysteresis due to the high H/C ratio of the samples. The different shape of voltage curves reflected the template effects on carbon. However, the practicality of these low-temperature carbons was severely limited because of the tested high capacity fade over merely a few cycles. Hence, further improvement in cycling capability of these new carbon materials is of great interest. In regard to microporous carbons, the template effect should be especially noted, because both the textures and surface properties of the as-synthesized product strongly depend on the templates employed. Textures and surface properties undoubtedly affect the electrochemical activity of electrode materials, which, however, still lacks of detailed investigations on the thermodynamics and kinetics of reversible Li storage. Moreover, micropores might hinder the electrolyte penetration and ionic diffusion to some extent and thus may be unfavorable to attain high-rate performance, as personally perceived.

Compared with microporous carbons, mesoporous carbons have been more extensively studied with respect to their application in lithium storage. Silica with mesopores was usually utilized as the templates to prepare mesoporous carbons. Herein two representative examples are given. Zhou and co-workers reported a high reversible capacity from ordered mesoporous carbon (CMK-3) that was synthesized using silica SBA-15 template.[52] Unprecedented electrochemical characteristics were observed from CMK-3, which possessed 3D ordered hexagonal structure with uniform pore size, high surface area, and large pore volume. They displayed a Li extraction potential in the range of 0.1–0.5 V, and delivered an initial capacity of 3100 mA h $g^{-1}$, corresponding to a lithiated composition of $Li_{8.4}C_6$. Reversible capacity of 850–1100 mA h $g^{-1}$ was also obtained. The enhanced electrode performance was believed to arise from the 3D ordered structure of CMK-3. Jiang's group also reported the synthesis of ordered 3D mesoporous carbons using similar method.[53] The as-obtained materials exhibited unusually high initial charge capacity and high kinetics at lower critical potential.

Three-dimensionally ordered macroporous (3DOM) carbons (as shown in Figure 5) have recently been synthesized using colloidal crystals of poly(methyl methacrylate) and inverse silica opal as the templates.[54,55] Applied as electrode materials in rechargeable lithium-ion batteries, these 3DOM structures exhibit several beneficial factors including (1) short diffusion length for $Li^+$, (2) numerous active sites for charge-transfer reactions, (3) reasonable electrical conductivity provided by the well interconnected walls, (4) high ionic conductivity of electrolyte through the carbon matrix, and (5) no need for binder and conducting additive. As reported by Stein and co-workers,[54] the prepared 3DOM carbon delivered 3 orders of magnitude greater discharge capacity than bulk carbon at elevated specific current, and possessed good cycling stability with only 17% reversible capacity fade after 30 cycles. The limited volumetric energy density stemming from high porosity was improved by coating $SnO_2$ on the surface of 3DOM carbon.[54] Similar work by Su et al. further confirmed the improvement of rate performance and cycling capability by using 3DOM carbon with a graphitic pore wall.[55]

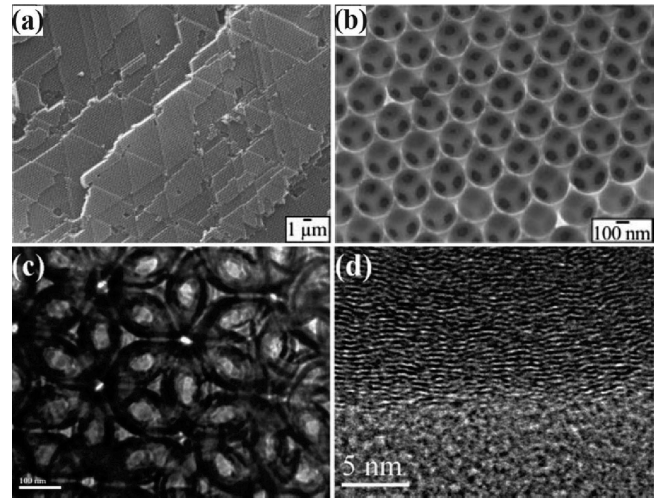


**Figure 5.** (a, b) SEM and (c, d) TEM images showing the morphologies of the template-prepared 3D ordered macroporous carbons. Adapted with permission from refs 54 and 55. Copyright 2005 Wiley and American Chemical Society, respectively.

The common characteristics of templated mesoporous and macroporous carbons are their well ordered 3D framework, uniform pore size, and high surface areas. The interconnectivity of the pore walls is another prominent morphology feature. In addition, hollow interior of porous carbons provide extra space for the electrolyte accommodation. These properties may facilitate electrolyte contact and electric and ionic diffusion/transfer and thereby result in a large capacity and favorable rate performance. One inherent disadvantage of porous structures is the low volumetric energy density. Coating with other high-specific-capacity components offers a promising strategy for relieving this hurdle, as demonstrated in the following examples of hybrid carbon materials.

**Hybrid Carbon Materials.** The template technique is a useful synthesis method to prepare nanocomposite structures, and thus offers the possibility of combing two or more types of functional materials into one incorporated entity for lithium storage. Recently, Zhao and co-workers reported an ordered, nanostructured tin-based oxides/carbon composite, which displayed better cycling performance than that of nanosized counterparts without carbon matrix.[56] Tin-based oxide was introduced into the pores of CMK-3 nanorods arrays with the aid of phosphorus ester. The prepared hybrid materials delivered an initial charge capacity of 1347 mA h $g^{-1}$ and a subsequent capacity of 515 mA h $g^{-1}$ when $Li^+$ extraction reactions proceeded up to 2 V. The superiority of the composite nanostructures were ascribed to three factors: (1) small grain size of tin-based oxides confined within the nanospaces of CMK-3 forbids the formation of two-phase Li-Sn alloys, (2) 3D interconnected carbon framework hinders particle aggregation, and (3) electronically conducting CMK-3 ensures good electrical contacts. Another example of composite structures is the carbon nanotubes bridged with mesoporous carbon particles.[57] To synthesize these hybrid materials, Su et al. deposited mesoporous carbon (OMC) and carbon nanotubes (CNT) sequentially inside the pores and on the external surfaces of SBA-15 template, respectively. The prepared OMC/

CNT composites exhibited enhanced cycling performance and rate capability, although their first capacity was lower than OMC without CNT decoration. The improved electrode performance of OMC/CNT hybrid materials was related to their much higher electrical conductivity as compared to that of OMC (i.e., 645 vs 138 S/m). Mui et al. also reported that nanocomposite electrode consisting of carbon nanotubes, gold, and block copolymer template matrix could cycle more than 600 times at rates varying between *C*/1.8 and 8.8*C* with little evidence of decrepitation and coarsensing.[58] However, for composite materials, the amount of the coated components should be optimized. Too much coating might increase the particle size and thereafter cause a barrier for ionic and electronic diffusion.

The above-mentioned examples indicate that structural and morphological characteristics of the templated carbon-based materials are beneficial to their electrochemical performance in rechargeable lithium-ion batteries. Template synthesis facilitates the formation of carbon materials with desired size, shape, crystalline structure, porosity, and chemical composition, which are all important factors affecting the electrochemical activities. Templated carbonaceous materials with ordered porous structure favor the enhancement of ionic diffusion, electrical conductivity, and electrolyte contact. Also, coating or decorating templated carbon materials with other active components may be helpful in further improving the related electrode performance.

## Metal Oxides

Metal oxides can adopt a large variety of structural geometries with an electronic structure that may exhibit metallic, semiconductor, or insulator characteristics, endowing them with diverse chemical and physical properties.[59] Metal oxides of novel morphologies, which were synthesized through the template route, have been investigated as attractive active materials for rechargeable lithium-ion batteries.[60–62] The emerging nanoscience and nanotechnology stimulate extensive research interest in nanostructured metal oxides for lithium storage.[63] It should be mentioned that the lithium-hosting possibility of nanostructured transition-metal dichalcogenides including $MoS_2$, $TiS_2$, $WS_2$ and so on has likewise attracted much attention, as clearly reviewed by Tenne.[64] Here, we highlight the recent progress in template-directed metal oxide nanostructures, mainly focusing on the most intensively studied oxides such as $SnO_2$, $Fe_2O_3$, $Co_3O_4$, $VO_x$, $MnO_x$, and $TiO_2$. The electrode mechanism of metal oxides is based on either lithium ion intercalation reaction or lithium conversion reaction. Some of the metal oxides are demonstrated to be suitable for negative active materials while others are promising positive electrode materials.

**Tin Oxide.** It has been shown that tin and tin-based oxides are promising candidates to replace the carbon-based anode materials because of their large theoretical capacity for lithium insertion (i.e., 990 mA h $g^{-1}$, supposed the formation of $Li_{4.4}Sn$ alloy) and safety benefit for avoiding the formation of hazardous Li dendrite.[9] The major drawback of applying these materials is the quick capacity fade caused by large volume expansion during the formation of Li−Sn alloys. Therefore, much attention has been paid to improve the cycling performance of tin oxides. Nanotubular, mesoporous, and nanocomposite $SnO_2$ materials are representative system developed in this direction.

A good example is the uniform polycrystalline $SnO_2$ nanotubes that have been fabricated through an infiltration route using $SnO_2$ nanoparticles as starting building units and AAO membranes as the template.[65] The as-obtained tubular $SnO_2$ showed a significant improvement of Li-insertion capacity and cycling life over the unorganized particle counterparts. A high specific capacity of 525 mA h $g^{-1}$ was attained after 80 cycles. These enhanced electrochemical characteristics were proposed to be associated with the unique features of $SnO_2$ polycrystalline nanotubes that follow: (1) Concentric expansion and contraction attainable from tubular organization of nanoparticles helps to relieve mechanical stress caused by electrode volume change; (2) Intra cavities, flexible thin walls, and open ends allow more efficient $Li^+$ transportation and insertion. A similar attempt using $SnO_2$ nanotubes to overcome the problem of rapid capacity fading was reported by Lee and his co-workers.[66] $SnO_2$ nanotubes with coaxially grown carbon-nanotube overlayers were prepared through a confined-space catalytic deposition process assisted by AAO membranes template. The obtained $SnO_2$-core/carbon-shell nanotubes exhibited highly reversible capacity (close to 600 mA h $g^{-1}$) and excellent cyclability with capacity retention of 92.5% after 200 cycles.

Surfactant-directed $SnO_2$-graphite nanostructured composites were also shown to deliver high reversible $Li^+$ storage capacity because of the uniform dispersion of $SnO_2$ nanoparticle on the graphite surface, which reduced particle aggregation during $Li^+$ insertion and extraction reaction.[67] The prominent novelty of the above composite materials stemmed from the synergistical combination of good electrically conductive carbon nanotubes and high-capacity $SnO_2$ nanotubes. Other form of $SnO_2$ 1D nanostructures such as nanofibers also showed extraordinarily improved rate capability and cycling performance because of the small grain size.[68]

Porous template-directed Sn-based materials have exhibited improved reversibility as well. $SnO_2$ nanocrystals with ordered mesoporous framework were prepared by using amphiphilic triblock copolymer as the template.[69] The obtained $SnO_2$ showed no aggregation of nanotin, high reversible capacity, and suppressed volume change. Another example directs to mesoporous tin samples, which delivered higher lithium extraction capacities than the nonporous tin.[70] The improvement was attributed to the ability of mesoporous tin to expand and contract with less structural degradation. The above examples indicate that the employment of templated tin or tin oxide structures, because of their unique morphological benefits, is helpful and effective to overcome the intrinsic problem of "electrode pulverization" existing in the charge and discharge process of Sn-based electrode.

**Iron/Cobalt-Based Oxides.** Interstitial-free 3d metal oxides have stimulated extensive research activities as anode electrode materials because of their considerably high specific capacities that arise from the conversion reactions with lithium. The reversible electrochemical reaction mechanism of these metal oxides is proposed to base on a displace redox

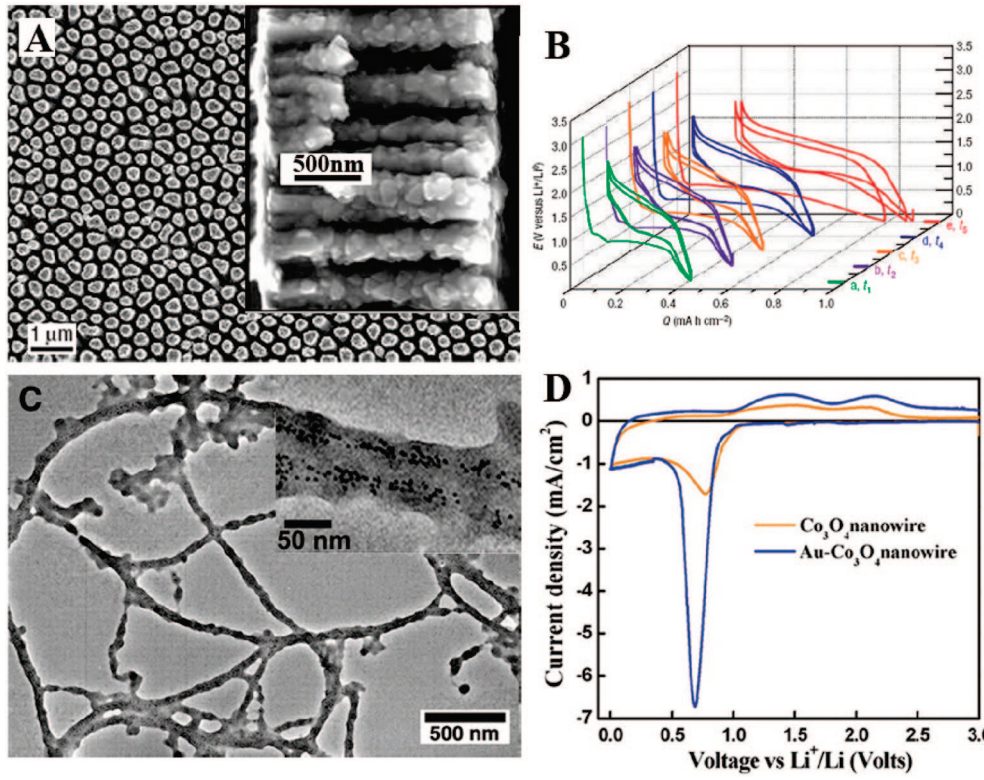


**Figure 6.** Transition-metal oxide nanostructures directed by the "hard" and "soft" template. (A) SEM images of the alumina membranes templated Cu current collector and the Cu nanostructures with $Fe_3O_4$ deposits (inset). (B) Potential−capacity profiles for the Cu-supported $Fe_3O_4$ deposits. (C) TEM images of the viruses-templated hybrid nanostructure of Au nanoparticles (inset) incorporated into $Co_3O_4$ nanowires. (D) Cyclic voltammograms of the hybrid Au−$Co_3O_4$ and $Co_3O_4$ nanowires. Adapted with permission from refs 30 and 72. Copyright 2006 American Association for the Advancement of Science and Nature Publishing Group, respectively.

reaction.[8] As a representative demonstration, the reactions occurring in $Fe_2O_3$ electrode (using metallic lithium as the counter electrode materials) can be described by

$$Fe_2O_3 + 6Li^+ + 6e^- \leftrightarrow 3Li_2O + 2Fe \text{ (cathode)}$$
$$6Li \leftrightarrow 6Li^+ + 6e^- \text{ (anode)}$$
$$Fe_2O_3 + 6Li \leftrightarrow 3Li_2O + 2Fe \text{ (overall)}$$

Reaction of $Fe_2O_3$ with Li is thermodynamically feasible; the formation of $Fe^0$ from $Fe^{3+}$ yields a theoretical capacity of 1007 mA h $g^{-1}$. Reverse extraction of Li from the $Li_2O$ matrix seems to be thermodynamically unattainable. However, nanosized electrode materials with a small particle size and a large proportion of surface atoms should possess high surface energy and enhance their electrochemical activity, making the back reaction possible when the electrode is charged. Similar mechanism of conversion reactions has been proposed in the cases of other nanostructured transition metal oxides such as NiO, CuO, $Co_3O_4$, and $MnO_2$.[8,24,63,71]

Special interests have been initiated by iron-based oxides such as $Fe_3O_4$ and $Fe_2O_3$ because of the advantages of low cost and low toxicity. Recently, Simon and his collaborators reported a $Fe_3O_4$-based Cu nanoarchitectured electrode for Li-ion batteries.[72] The electrode was prepared by using a two-step design: the electrochemically assisted template growth of Cu nanorods followed by electrodeposition of $Fe_3O_4$ (Figure 6A). The obtained nanostructured electrodes were demonstrated to show a factor of 6 improvement in power density over planar electrodes. High capacity as well as excellent rate capability and cycling performance were also observed, making these conversion electrodes attractive to traditional intercalation electrodes for Li-ion batteries. In addition, large hysteresis between charge and discharge profiles was presented in the conversion reactions (Figure 6B), which was suggested to derive from the high activation barrier triggering the oxidation and reduction reactions. This charge/discharge potential difference, however, would result in poor energy efficiency and thus remains to be overcome as one of the major hurdles in the applicability of $Fe_3O_4$ nanoarchitectures.

Similar to iron oxides, cobalt oxides such as CoO and $Co_3O_4$ have shown excellent electrochemical performance based on lithium conversion reactions. Intensive research interest has been gained in the synthesis, assembly, and application of $Co_3O_4$ nanostructures with diverse morphologies such as particle, tube, wire, and rod. A recent significant progress made in this field was reported by Belcher and coworkers.[30] Viruses were introduced as the template to synthesize and assemble $Co_3O_4$ and hybrid Au−$Co_3O_4$ nanowires (Figure 6C) under ambient and aqueous conditions. The virus-prepared crystalline $Co_3O_4$ nanowires exhibited higher reversible capacity than powders without viruses. The superior electrochemical properties of the viral templated wires were ascribed to their large surface areas, structural integrity, and dense packing, as well as favorable crystallinity. Hybrid nanostructures, namely, Au nanoparticles incorporated into $Co_3O_4$ nanowires, could generate even higher reversible lithium storage capacity (Figure 6D) exceeding 1000 mA h $g^{-1}$. This enhancement was associated with the dispersive Au nanoparticles that possessed high

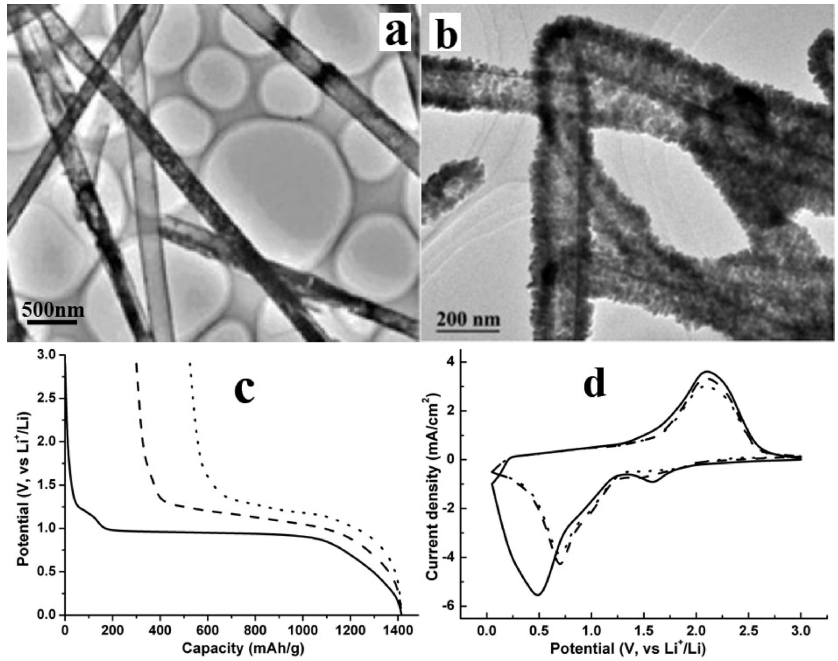


**Figure 7.** TEM images of the templated α-$Fe_2O_3$ nanotubes (a) before and (b) after 100 charge/discharge cycles; (c) discharge curves and (d) CVs of the nanotube electrode at the first (solid), 10th (dash), and 20th (dotted) cycles. Adapted with permission from ref 24a. Copyright 2005 Wiley.

electronic conductivity and possible catalytic effects on the Li conversion reaction. The template technique can be extended to construct large-length-scale 2D organized nanowire films, which sustain high capacity and excellent high-rate cycling capability as well. Therefore, virus-based template synthesis provides a valuable platform for integrating nanostructured electrode materials to design high-power and flexible lithium batteries.

$Fe_2O_3$ and $Co_3O_4$ nanotubes were prepared by thermal decomposition of iron and cobalt nitrate precursors within the pores of AAO membranes.[24] Uniform nanotubes with open-ended tips were obtained after template removal (Figure 7a). The length and diameter of the tubes corresponded well with the membrane thickness and the pore size of the template, respectively, confirming the efficiency of the template-assisted route with thermal decomposition to synthesize transition metal oxide nanostructures. The tube body is straight and the tube wall is composed of many nanoparticles. These characters resemble that mentioned in the above case of $SnO_2$ nanotubes and thus superior electrochemical activity can be expected.[65,66] The results of cyclic voltammograms (CVs) and electrochemical charge/discharge curves (Figure 7c,d) indeed revealed excellent electrode performance. In the case of $Fe_2O_3$ nanotubes, a capacity of 510 mA h $g^{-1}$ was attained after 100 cycles, which was much higher than that of graphite.[24a] As to $Co_3O_4$ nanotubes, longer plateau and reduced capacity fade were examined in comparison with their rod and particle counterparts.[24b] TEM image (Figure 7b) after several discharge/charge cycles indicated that the basic 1D morphology of the electrode materials was preserved. Interestingly, an agglomeration of very fine particles can be found around the wall of $Fe_2O_3$ tubes. The observed nanosize particles, which were produced in situ after the first discharge, confirm the proposed mechanism of conversion reaction and are indicative of the electrochemical activity of nanotubes. Hence, these results again suggest that the templated tubular nanostructures are beneficial to gaining superior electrochemical characteristics.

With respect to the conversion reactions of transition metal oxide, polarization remains to be a major problem. The reverse extraction of lithium from $Li_2O$ is thermodynamically unfavorable, leading to irreversibility of the electrochemical process. Experimentally, capacity fade usually occurs although the initial capacity value is considerably high. Another disadvantageous factor is the particle agglomeration, which may not only block the electrolyte accessibility but also cause activity deterioration on electrode materials. Templated 1D metal oxide nanostructures especially nanotubes that are composed of binding nanosize grains should outperform the bulk counterparts and monodispersive particles in that the nanostructure can be better retained after cycling. Furthermore, since temperature is an important factor for triggering the energetic barrier and thereby for lowering the polarization of conversion reactions,[72] application of these electrode materials under severe conditions (e.g., tropical district) may be of some interest.

**Titanium Oxide.** There is much current interest in investigating the lithium storage properties of nanotubes and nanowires based on titanium oxide or titanate because of their prominent advantages such as high capacity, good kinetic characteristics, good robustness and safety, wide availability, and low toxicity.[73] $TiO_2$ nanowires and nanotubes have been demonstrated to be promising anode materials for rechargeable lithium batteries.[74] Self-assembled organic surfactant is the most widely employed template to prepare titanium oxide nanostructures. However, to the best of our knowledge, the application of template-synthesized $TiO_2$ nanostructures in lithium storage has been seldom reported despite the extensive study on their synthesis.

Kavan et al. characterized the lithium insertion electrochemistry in organized anatase.[75] Mesoporous anatase was

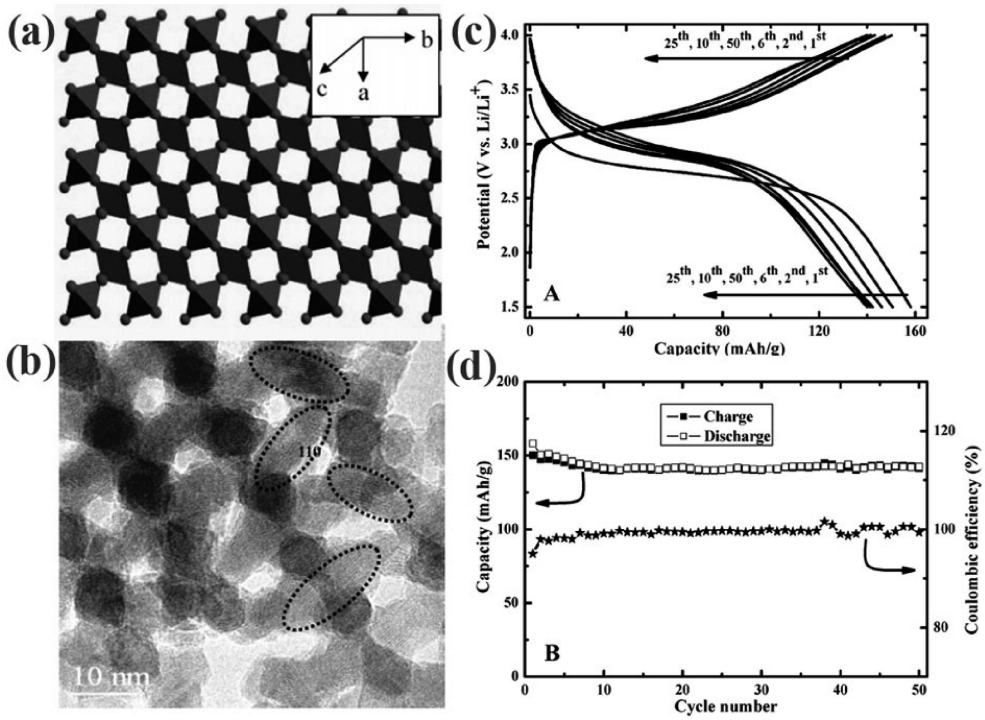


**Figure 8.** (a) Structure of $\beta$-$MnO_2$ with [1 × 1] tunnels, (b) high-resolution TEM image along the [210] direction, (c) charge and discharge curves, and (d) cycling performance and Coulombic efficiency of the templated mesoporous $\beta$-$MnO_2$. Adapted with permission from ref 78. Copyright 2006 American Chemical Society.

prepared by hydrolysis of $TiCl_4$ in the presence of poly(alkylene oxide) block copolymer as the template. Electrochemical studies in $Li^+$ containing organic electrolyte revealed that the thin layer electrodes of highly organized nanotextured anatase showed unusually fast capacitive and Li-insertion charging. Another surprising finding was that two new pairs of peaks were observed in CVs, in addition to the normal peaks of Li insertion.[75a] These so-called S-peaks indicated the mesoscopic ordering of the templated $TiO_2$ skeleton and were suggested to be correlated with the presence of amorphous $TiO_2$ in the electrode. Thus, the template has prominent effect on the electrochemical behaviors of $TiO_2$ materials. A recent study on the lithium insertion into templated $TiO_2$ nanostructure from aqueous solution was reported by Owen and co-workers.[76] The nanostructured $TiO_2$ films obtained via the template route were found to be reduced when they were cathodically polarized in aqueous lithium hydroxide, unlike the films synthesized without surfactant template. The porous nanostructures facilitated the solid-state reaction kinetics of Li ion insertion and diffusion. Rapidly reversible insertion of $Li^+$ in the electrode could result in the formation of $Li_{0.27}TiO_2$. However, fast self-discharge was inevitable when applying $TiO_2$ nanostructures to lithium storage in aqueous electrolyte. The favorable Li-insertion characteristics of template-mediated nanostructured $TiO_2$ film may be especially valuable for promising application in high-power aqueous supercapacitors rather than in batteries.

**Manganese Oxide.** Manganese oxides possess diverse layered or tunneled structures and can be used as positive active materials for lithium-based batteries. Templated $MnO_2$ nanostructures have demonstrated enhanced electrochemical properties than the bulk counterparts. For example, $MnO_2$ nanofibers were fabricated by combining template-based method and sol–gel chemistry.[77] The templated fiber with controllable dimensions possessed an $\alpha$-$MnO_2$ polymorph with hollandite-type structure. They delivered a first capacity of 183 mA h $g^{-1}$ and a stabilized capacity of 134 mA h $g^{-1}$ on the tenth cycle, under a cycling potential range between 2 and 3.5 V. As a comparison, bulk $MnO_2$ typically exhibited capacity no more than 120 mA h $g^{-1}$. Higher capacity values of the nanofirbers over their bulk counterparts were proposed to be derived from the large surface areas of the nanosized materials.

A recent work by Xia and co-workers reported a highly electrochemical reaction of lithium in the template-prepared mesoporous $\beta$-$MnO_2$, which has been generally believed to exhibit poor electrode performance due to the highly crystallinity and crystal structure with narrow channels.[78] The well-ordered mesoporous $MnO_2$ were prepared using silica KIT-6 as the template by thermal decomposition of $Mn(NO_3)_2$. XRD analysis and TEM images along different axes revealed that the synthesized $MnO_2$ replicated the mesoporous structure of KIT-6 silica template with similar dimension of cubic unit cell (Figure 8). From morphological and textural characterization, the mesoporous materials possessed rougher surface, smaller particle size, and much larger surface areas than those of conventional bulk form. A pair of redox peaks at 2.6 and 3.2 V was detected on the CV curves of templated $\beta$-$MnO_2$, demonstrating much higher peak current density than the conventional counterparts. Also, the mesoporous $MnO_2$ exhibited flat discharge/charge plateaus, considerably large capacity, as well as pretty good cycling performance and Coulombic efficiency (Figure 8c and d). These significantly improved electrode performances over highly crystalline $\beta$-$MnO_2$ were proposed to stem from the ordered mesoporous

structure. Ionic diffusion and transport is not favorable in conventional $\beta$-$MnO_2$ because of the narrow [1 × 1] channels (Figure 8a) and large particle size, whereas the templated $MnO_2$ provides mesoporous void between the nanosized pore walls, facilitating the interfacial $Li^+$ transfer and intercalation (Figure 8b). The ordered mesopores decrease the effective diffusion path and increase the surface area for insertion and extraction of $Li^+$, and meanwhile act as a buffer between the blocks to alleviate the volume expansion caused by repeated ionic intercalation. Therefore, the templated mesoporous structures resulted in uncommon enhanced electrochemical characteristics for $\beta$-$MnO_2$.

The significantly enhanced electrochemical performance of templated mesoporous $\beta$-$MnO_2$ over the bulk crystalline counterparts has been confirmed by Jiao and Bruce.[79] On the basis of their report, the template-directed $\beta$-$MnO_2$ with a highly ordered pore structure and highly crystalline walls can accommodate reversibly a large amount of Li (Li:Mn = 0.92:1) on intercalation, with more than 80% capacity retention after cycling at a high rate of 300 mA $g^{-1}$ for 50 cycles. Surprisingly, TEM and XRD analysis indicated that both the ordered porous morphology and the crystal structure were preserved on cycling. As a sharp contrast, the rapid conversion of $\beta$-$MnO_2$ to $LiMn_2O_4$ spinel phase occurred during chemical intercalation of lithium into bulk $MnO_2$.[79] The greatly improved electrochemical activity was again proposed to derive from the ordered thin walls of the templated structures that could accommodate the volume changes during repeated lithium intercalation. In the above examples of templated $MnO_2$, we note that the cutoff voltage was set above 1.5 V. However, in another example of $MnO_2$ nanowires, the assembled electrode was charged and discharged between 0.01 to 2 V vs $Li^+$/Li, where reversible capacity of 800 mA h $g^{-1}$ was achieved, making them potential anode materials.[71b] Presumably, this markedly inconsistent electrochemical behavior arises from the different mechanism between lithium insertion and conversion reactions. It may be attractive to further investigate the electrode performance of template-directed $MnO_2$ nanostructures when cycling in a lower voltage range.

**Vanadium Oxide.** Vanadium oxides such as $V_2O_5$ and $VO_x$ are typical intercalation compounds with layered structure to host guest molecules, and especially display high positive redox potential for Li insertion. Vanadium oxide nanostructures have received wide research interests in terms of their synthesis and lithium-ion intercalation properties for energy storage.[80] In particular, the template synthesis of vanadium pentoxide ($V_2O_5$) 1D nanostructures with enhanced properties of Li-intercalation has been recently reported. Early work was carried out by Spahr et al. on the preparation of redox-active vanadium oxide nanotubes by using alkylamine surfactants as the template.[81] Patrissi and Martin later reported on the synthesis of orthorhomibic $V_2O_5$ nanofibers using polycarbonate (PC) membranes template and the study of their rate performance for Li intercalation.[82] Whittingham and co-workers recently employed a polylactide fiber template-directed process to prepare vanadium oxide $V_2O_5$ with novel fibrous and tubular morphology.[83] The fibrous nanomorphology was believed to provide shorter diffusion length, reduce the stress in the vanadium oxide compound, and allow structure maintenance, thus leading to improved electrochemical performance over bulk $V_2O_5$. Another example also showed that $V_2O_5$ nanofibers can deliver dramatically higher specific discharge capacities than micrometer-sized $V_2O_5$ fibers.[84] In addition, significantly enhanced low-temperature performance with decreased particle size was obtained for these nanostructured electrode materials. Cao and collaborators prepared and electrochemically investigated different template-prepared $V_2O_5$ nanostructures including nanorods and nanotubes arrays as well as Ni-$V_2O_5 \cdot nH_2O$ core–shell nanocable arrays.[85–87] More recently, the electrochemical and structural aspects of lithium insertion into vanadium oxide nanotubes were systematically studied.[88]

Single-crystal $V_2O_5$ nanorods were obtained over a large area with near unidirectional alignment via electrochemical deposition, being assisted by porous PC template.[85] Current–voltage curves suggested that both nanorods and the comparative sol–gel-derived films underwent similar phase changes, whereas the former possessed much lower Li diffusion resistance than the latter. For a given current density, the templated nanorod arrays could deliver approximately five times higher Li insertion capacity. The different electrochemical performance was ascribed to the difference in microstructures. The nanorod arrays were composed of vanadia layers in parall to the rod axis, which favored the $Li^+$ intercalation and extraction because reactions occurred along the side surface of rods and the solid-state diffusion distance was very small. As a comparison, polycrystalline sol–gel $V_2O_5$ films consisted of platelet vanadia grains, where charge transport and $Li^+$ insertion/extraction was retarded because of the existing crystal grains and grain boundaries. In addition, $V_2O_5$ nanotubes arrays delivered an initial capacity of 300 mA h $g^{-1}$ and a stabilized capacity of 160 mA h $g^{-1}$, much higher than that of $V_2O_5$ films.[86] Moreover, the template-directed nanocables arrays with $V_2O_5 \cdot nH_2O$ shell and Ni core exhibited further enhanced $Li^+$ intercalation characteristics over the single-crystal naorods.[87] At least 1 order of magnitude higher energy and power density was attained with the core–shell nanostructures in comparison to the sol–gel film electrode.

More recently, Nordlinder et al. prepared $VO_x$ nanotubes by employing cost-effective crystalline $V_2O_5$ as the precursor and dodecylamine ($C_{12}H_{25}NH_2$) as the structure-directing agent.[88] Ca-$VO_x$ nanotubes were also synthesized through ion exchange. The authors presented in their report the systematical investigation of the Li-intercalation mechanism into the $VO_x$ nanotubes and the structural change occurring in electrode reactions. It was found that to maintain reversible and large capacity for the nanotubes, the low potential limit must be set below 1.5 V but not lower than 1.3 V because a too cathodic potential limit might induce phase transitions and thus considerably reduce the electrode performance. Electrochemical measurements and in situ XRD results indicated that at least two processes occurs for $Li^+$ intercalation into the $VO_x$ nanotubes: a fast $Li^+$ insertion between the $VO_x$ layers and a subsequent slow diffusion and residence of $Li^+$ in the interlayer spacing. The $Li^+$ insertion process occurs in a disordered way and leads to decreased interlayer

**Table 1. Summary of the Representative Template-Directed Electrode Materials for Lithium Storage**

| product | template employed | structure & morphology | merits for lithium storage | ref |
|---|---|---|---|---|
| C | SBA-15 | 3D ordered mesoporous | reversible capacity 850–1100 mA h $g^{-1}$ | 52 |
| C | colloidal crystal/silica opal | 3D ordered macroporous | short diffusion length<br>more active sites<br>high conductivity | 54·55 |
| C/SnO | CMK-3 | ordered composite | small grain size<br>reduced particle aggregation | 56 |
| $SnO_2$ | AAO | nanotube | tubular flexibility<br>intracavities<br>thin walls/open ends | 65 |
| $Fe_3O_4$ | AAO | $Fe_3O_4$−Cu nanorod | high power density<br>capacity retention | 72 |
| Au-$Co_3O_4$ | viruses | assembled nanowire | large surface area<br>structural integrity<br>Au catalytic effect | 30 |
| $TiO_2$ | surfactant | porous film | rapid aqueous $Li^+$ insertion | 76 |
| $\beta$-$MnO_2$ | KIT-6 | 3D ordered mesoporous | enhanced capacity<br>improved cyclability<br>rate capability | 78·79 |
| $V_2O_5$ | AAO/PC | nanotube/rod/cable | capacity >160 mA h $g^{-1}$<br>lower diffusion resistance | 85−87 |
| $LiCoO_2$ | SBA-15/KIT-6 | nanowire/mesoporous | less fade in capacity | 34 |
| $Li_4Ti_5O_{12}$ | colloidal crystal | 3D ordered macroporous | high $Li^+$ conductivity<br>electrolyte accessibility<br>facilitated $Li^+$ diffusion | 42·43 |

distance; the slower process causes two-dimensional relaxation of the structure within the $VO_x$ layers. During lithium insertion, vanadium was reduced from high valence to lower oxidation state, resulting in an increase in its coordination number and changes in cell parameters. Significant alteration in crystal structure might be induced if a two large amount of lithium was inserted.

These results thereby suggest that careful control of the charge/discharge potential range is necessary to attain satisfactory electrode performance with $VO_x$ nanomaterials. Moreover, vanadium oxide materials are abundant with valence, composition, structure, and morphology, which strongly affect the electrode properties such as voltage profile, capacity, and rate performance. For instance, low crystalline $V_2O_5$ containing a certain amount of water were found to exhibit higher $Li^+$-intercalation capacity and more sustainable cycling life than the anhydrous crystalline forms.[80b] Further research interests will continue in the direction of vanadium-based oxides because of their advantages of being cheap and easy to prepare and offering high energy density.

## Conclusion and Outlook

The template technique offers an effective way for controlled preparation of electrode materials and thus makes it possible to better understand the effects of structure, morphology, and composition on the electrochemical properties. A variety of template-directed materials have been demonstrated to improve the performance of rechargeable Li-ion batteries. Table 1 summarizes some of the typical template synthesis of electrode materials. Compared to those materials with traditional forms, the general benefits of employing templated materials for lithium storage can be highlighted as follows. First, templated materials are usually associated with small grain size and high surface area. Decreased particle size shortens the transportation/diffusion path for both electrons and ions, thus leading to faster kinetics. Second, high surface area favors the efficient contact between active materials and electrolytes, providing more active sites for electrochemical reactions. Third, template synthesis can result in well-controlled structures with porosity and interconnectivity, which supply extra accessible space for lithium ions while maintaining sufficient conductivity for solid electronic transfer. Significantly enhanced capacity and high rate capability can be thus expected. Moreover, template-directed materials possess favorably morphological stability, which helps to alleviate the structure damage caused by volume expansion during the cycling process. In many cases, such as nanotubes or 3D porous structures, the basic morphology is preserved after numerous cycles. Hence, improved cycling capability can be obtained by using template-prepared materials.

In view of the emerging application of nanomaterials, the template technique is not only a valuable synthesis route to attain desired nanostructures but also a powerful strategy to fabricate nanostructured active materials into an electrode, which maintains the benefits of electrochemistry at the nanoscale. During the electrode assembly process, nanosize active materials usually need to be mixed with additive or coated on current collector, leading to the formation of electrode film. As a result, the beneficial gains from the small particle size may be negated to some extent. Other penalties may arise from the unfavorable interfaces. Template processing provides a possibility of using 3D architectured electrode, which consists of both nanoscale active materials and supporting matrix (as the current collector) without traditional electrode assembly process.[89] Such 3D electrodes will be particularly useful in constructing microbatteries.[90] Another prominent advantage of template synthesis is that, as demonstrated in many cases, it enables the systematic and controlled arrangement of two or more active materials, which can enhance the electrode performance through the cooperative contribution of each component.

Apart from the prominent advantages of template-prepared electrode materials, there are also some intrinsic drawbacks hindering their practical applications. The major problem is the limitation to large-scale synthesis. Mass production of templates with controlled structures is first of all not easy. The cost caused by the template itself and the commonly required postsynthesis procedures (e.g., template removal) may make the manipulation of template preparation costly, complicated, or even uneconomical. Moreover, templated electrode materials usually demonstrate low specific volumetric energy because of the void nature of templates. Indeed, efforts have already been dedicated to overcoming these hurdles. For example, coating with high-capacity materials and increasing the porosity density of templates can improve the volumetric specific energy. Of course, further work is still required in this direction. On the other hand, the reaction mechanism of template-directed nanostructures remains unclear in many cases. There is also a challenge in better understanding the unique behaviors of templated electrode materials from the perspective of both thermodynamics and kinetics. More theoretical and experimental work in this aspect will be attractive and of special importance.

Considering the outstanding superiority over other types of batteries, rechargeable lithium-ion batteries are very likely to continue their dominating position in the power source market for portable devices in the near future or even extending to the next decade. Another massive market force is expected to develop in the area of microelectromechanical systems that require microscaled power-devices. There may be also a chance for rechargeable lithium-ion batteries to power electric vehicles, which are future alternative to current gasoline-fueled cars. Template-prepared active materials may offer further opportunities to design new-type batteries with improved characteristics including more flexible shape and higher specific capacity and energy density, as well as longer cycling life. Finally, we believe that templated electrode materials will not only stimulate research curiosity but also find practical application in rechargeable lithium-ion batteries with the advancement of modern materials science and technology.

**Acknowledgment.** This work was supported by National NSFC (20325102 and 20703026) and 973 Program (2005CB623607).

## References

(1) Whittingham, M. S. *Chem. Rev.* **2004**, *104*, 4271.
(2) Tarascon, J. M.; Armand, M. *Nature* **2001**, *414*, 359.
(3) Linden, D.; Reddy, T. B. *Handbook of Batteries*, 3rd ed.; McGraw-Hill: New York, 2002.
(4) Kang, K.; Meng, Y. S.; Bréger, J.; Grey, C. P.; Geder, G. *Science* **2006**, *311*, 977.
(5) Winter, M.; Besenhard, J. O.; Spahr, M. E.; Novák, P. *Adv. Mater.* **1998**, *10*, 725.
(6) (a) Sato, K.; Noyuchi, M.; Demachi, A.; Oki, N.; Endo, M. *Science* **1994**, *264*, 556. (b) Dahn, J. R.; Zheng, T.; Liu, Y.; Xue, J. S. *Science* **1995**, *270*, 590.
(7) Tirado, J. L. *Mater. Sci. Eng., R* **2003**, *40*, 103.
(8) Poizot, P.; Laruelle, S.; Grugeon, S.; Dupont, L.; Tarascon, J. M. *Nature* **2000**, *407*, 496.
(9) Idota, Y.; Kubota, T.; Matsufuji, A.; Maekawa, Y.; Miyasaka, T. *Science* **1997**, *276*, 1395.
(10) Padhi, A. K.; Nanjundaswamy, K. S.; Goodenough, J. B. *J. Electrochem. Soc.* **1997**, *144*, 1188.
(11) Chung, S. Y.; Bloking, J. T.; Chiang, Y. M. *Nat. Mater.* **2002**, *1*, 123.
(12) Aricò, A. S.; Bruce, P.; Scrosati, B.; Tarascon, J. -M.; Schalkwijk, W. V *Nat. Mater.* **2005**, *4*, 366.
(13) (a) Liu, H. K.; Wang, G. X.; Guo, Z. P.; Wang, J. Z.; Konstantinov, K. *J. Nanosci. Nanotechnol.* **2006**, *6*, 1. (b) Panero, S.; Scrosati, B.; Wachtler, M.; Croce, F. *J. Power Sources* **2004**, *129*, 90.
(14) Cheng, F. Y.; Chen, J. *J. Mater. Res.* **2006**, *21*, 2744.
(15) Lin, H. P.; Mou, C. Y. *Acc. Chem. Res.* **2002**, *35*, 927.
(16) Schüth, F. *Angew. Chem., Int. Ed.* **2003**, *42*, 3604.
(17) van Bommel, K. J. C.; Friggeri, A.; Shinkai, S. *Angew. Chem., Int. Ed.* **2003**, *42*, 980.
(18) Valdés-Solís, T.; Fuertes, A. B. *Mater. Res. Bull.* **2006**, *41*, 2187.
(19) (a) Martin, C. R. *Science* **1994**, *266*, 1961. (b) Lakshmi, B. B.; Patrissi, C. J.; Martin, C. R. *Chem. Mater.* **1997**, *9*, 2544. (c) Nishizawa, M.; Mukai, K.; Kuwabata, S.; Martin, C. R.; Yoneyama, H. *J. Electrochem. Soc.* **1997**, *144*, 1923.
(20) Sides, C. R.; Li, N. C.; Patrissi, C. J.; Scrosati, B.; Martin, C. R. *MRS Bull.* **2002**, *27*, 604.
(21) Zakhidov, A. A.; Baughman, R. H.; Iqbal, Z.; Cui, C.; Khayrullin, I.; Dantas, S. O.; Marti, J.; Ralchenko, V. G. *Science* **1998**, *282*, 897.
(22) Schneider, J. J.; Engstler, J. *Eur. J. Inorg. Chem.* **2006**, 1723.
(23) (a) Sun, Y.; Tao, Z.; Chen, J.; Herricks, T.; Xia, Y. *J. Am. Chem. Soc.* **2004**, *126*, 5940. (b) Chen, J.; Tao, Z.; Li, S. *J. Am. Chem. Soc.* **2004**, *126*, 3060.
(24) (a) Chen, J.; Xu, L.; Li, W.; Gou, X. *Adv. Mater.* **2005**, *17*, 582. (b) Li, W. Y.; Xu, L. N.; Chen, J. *Adv. Funct. Mater.* **2005**, *15*, 851.
(25) (a) Cai, F. S.; Zhang, G. Y.; Chen, J.; Gou, X. L.; Liu, H. K.; Dou, S. X. *Angew. Chem., Int. Ed.* **2004**, *43*, 4212. (b) Cheng, F. Y.; Chen, J.; Shen, P. W. *J. Power Sources* **2005**, *150*, 255. (c) Li, W.; Zhang, S.; Chen, J. *J. Phys. Chem. B* **2005**, *109*, 14025.
(26) Li, X.; Cheng, F.; Guo, B.; Chen, J. *J. Phys. Chem. B* **2005**, *109*, 14017.
(27) Zhang, G.; Li, C.; Cheng, F.; Chen, J. *Sens. Actuators, B* **2007**, *120*, 403.
(28) Gin, D. L.; Gu, W.; Pindzola, B. A.; Zhou, W. J. *Acc. Chem. Res.* **2001**, *34*, 973.
(29) Gou, X.; Cheng, F.; Shi, Y.; Zhang, L.; Peng, S.; Chen, J.; Shen, P *J. Am. Chem. Soc.* **2006**, *128*, 7222.
(30) Nam, K. T.; Kim, D. W.; Yoo, P. J.; Chiang, C. Y.; Meethong, N.; Hammond, P. T.; Chiang, Y. M.; Belcher, A. M. *Science* **2006**, *312*, 885.
(31) Polarz, S.; Antonietti, M. *Chem. Commun.* **2002**, 2593.
(32) Amatucci, G. G.; Tarascon, J. M.; Klein, L. *J. Electrochem. Soc.* **1996**, *143*, 1114.
(33) Liao, C. L.; Wu, M. T.; Yen, J. H.; Leu, I. C.; Fung, K. Z. *J. Alloys Compds.* **2006**, *414*, 302.
(34) Jiao, F.; Shaju, K. M.; Bruce, P. G. *Angew. Chem., Int. Ed.* **2005**, *44*, 6550.
(35) Fonseca, C. P.; Fantini, M. C. A.; Neves, S. *Thin Solid Films* **2005**, *488*, 68.
(36) Fonseca, C. P.; Paula, R. M.; Pallone, E. M. J. A.; Neves, S. *Electrochim. Acta* **2006**, *51*, 6419.
(37) Wu, Q.; Li, W.; Cheng, Y.; Jiang, Z. *Mater. Chem. Phys.* **2005**, *91*, 463.
(38) Yang, S.; Yue, H.; Yin, Y.; Yang, J.; Yang, W. *Electrochim. Acta* **2006**, *51*, 4971.
(39) Zhou, Y.; Shen, C.; Li, H. *Solid State Ionics* **2002**, *146*, 81.
(40) Bullock, S. E.; Kofinas, P. *J. Power Sources* **2004**, *132*, 256.
(41) Liu, X.; Wang, J.; Zhang, J.; Yang, S. *J. Mater. Sci: Mater. Electron.* **2006**, *17*, 865.
(42) (a) Kanamura, K.; Akutagawa, N.; Dokko, K. *J. Power Sources* **2005**, *146*, 86. (b) Rho, Y. H.; Kanamura, K. *J. Power Sources* **2006**, *158*, 1436. (c) Dokko, K.; Sugaya, J.; Nakano, H.; Yasukawa, T.; Matsue, T.; Kanamura, K. *Electrochem. Commun.* **2007**, *9*, 857.
(43) Sorensen, E. M.; Barry, S. J.; Jung, H. K.; Rondinelli, J. R.; Vaughey, J. T.; Poeppelmeier, K. R. *Chem. Mater.* **2006**, *18*, 482.
(44) (a) Sato, K.; Noyuchi, M.; Demachi, A.; Oki, N.; Endo, M. *Science* **1994**, *264*, 556. (b) Dahn, J. R.; Zheng, T.; Liu, Y.; Xue, J. S. *Science* **1995**, *270*, 590.
(45) Tirado, J. L. *Mater. Sci. Eng., R* **2003**, *40*, 103.
(46) Ajayan, P. M. *Chem. Rev.* **1999**, *99*, 1787.
(47) Rao, C. N. R.; Satishkumar, B. C.; Govindaraj, A.; Nath, M. *ChemPhysChem* **2001**, *2*, 78.
(48) Che, G.; Lakshmi, B. B.; Fisher, E. R.; Martin, C. R. *Nature* **1998**, *393*, 346.
(49) Li, N. C.; Mitchell, D. T.; Lee, K. P; Martin, C. R *J. Electrochem. Soc.* **2003**, *150*, A979.
(50) (a) Habazaki, H.; Sato, S.; Habazaki, H.; Inagaki, M. *Carbon* **2004**, *42*, 2756. (b) Habazaki, H.; Kiriu, M.; Konno, H. *Electrochem. Commun.* **2006**, *8*, 1275.
(51) Meyers, C. J.; Shah, S. D.; Patel, S. C.; Sneeringer, R. M.; Bessel, C. A.; Dollahon, N. R.; Leising, R. A.; Takeuchi, E. S. *J. Phys. Chem. B* **2001**, *105*, 2143.
(52) Zhou, H.; Zhu, S.; Hibino, M.; Honma, I.; Ichihara, M. *Adv. Mater.* **2003**, *15*, 2107.
(53) Wang, T.; Liu, X.; Zhao, D.; Jiang, Z. *Chem. Phys. Lett.* **2004**, *389*, 327.
(54) Lee, K. T.; Lytle, J. C.; Ergang, N. S.; Oh, S. M.; Stein, A. *Adv. Funct. Mater.* **2005**, *15*, 547.
(55) Su, F.; Zhao, X. S.; Wang, Y.; Zeng, J.; Zhou, Z.; Lee, J. Y. *J. Phys. Chem. B* **2005**, *109*, 20200.
(56) Fan, J.; Wang, T.; Yu, C.; Tu, B.; Jiang, Z.; Zhao, D. *Adv. Mater.* **2004**, *16*, 1432.
(57) Su, F.; Zhao, X.; Wang, Y.; Lee, J. Y. *Microporous Mesoporous Mater.* **2007**, *98*, 323.

(58) Mui, S. C.; Trapa, P. E.; Huang, B.; Soo, P. P.; Lozow, M. I.; Wang, T. C.; Cohen, R. E.; Mansour, A. N.; Mukerjee, S.; Mayes, A. M.; Sadoway, D. R. *J. Electrochem. Soc.* **2002**, *149*, A1610.
(59) Fernández-García, M.; Martínez-Arias, A.; Hanson, J. C.; Rodriguez, J. A. *Chem. Rev.* **2004**, *104*, 4063.
(60) Rumplecker, A.; Kleitz, F.; Salabas, E. L.; Schüth, F. *Chem. Mater.* **2007**, *19*, 485.
(61) Yue, W.; Zhou, W. *Chem. Mater.* **2007**, *19*, 2359.
(62) Li, H.; Huang, X.; Chen, L. *Solid State Ionics* **1999**, *123*, 189.
(63) (a) Obrovac, M. N.; Dunlap, R. A.; Sanderson, R. J.; Dahn, J. R. *J. Electrochem. Soc.* **2001**, *148*, A576. (b) Nazar, L. F.; Goward, G.; Leroux, F.; Duncan, M.; Huang, H.; Kerr, T.; Gaubicher, J. *Int. J. Inorg. Mater.* **2001**, *3*, 191.
(64) (a) Tenne, R. *Nat. Nanotechnol.* **2006**, *1*, 103. (b) Tenne, R. *J. Mater. Res.* **2006**, *21*, 2726. (c) Tenne, R. *Angew. Chem., Int. Ed.* **2003**, *42*, 5124.
(65) Wang, Y.; Lee, J. Y.; Zeng, H. C. *Chem. Mater.* **2005**, *17*, 3899.
(66) Wang, Y.; Zeng, H. C.; Lee, J. Y. *Adv. Mater.* **2006**, *18*, 645.
(67) Wang, Y.; Lee, J. Y.; Chen, B. H. *Electrochem. Solid State Lett.* **2003**, *6*, A19.
(68) (a) Li, N. C.; Martin, C. R.; Scrosati, B. *J. Power Sources* **2001**, *97–98*, 240. (b) Li, N. C.; Martin, C. R. *J. Electrochem. Soc.* **2001**, *148*, A164.
(69) Wang, T.; Ma, Z.; Xu, F.; Jiang, Z. *Electrochem. Commun.* **2003**, *5*, 599.
(70) Whitehead, A. H.; Elliott, J. M.; Owen, J. R. *J. Power Sources* **1999**, *81–82*, 33.
(71) (a) Needham, S. A.; Wang, G. X.; Liu, H. K. *J. Power Sources* **2006**, *159*, 254. (b) Wu, M. S.; Chiang, P. C. J.; Lee, J. T.; Lin, J. C. *J. Phys. Chem. B* **2005**, *109*, 23279.
(72) Taberna, P. L.; Mitra, S.; Poizot, P.; Simon, P.; Tarascon, J. -M. *Nat. Mater.* **2006**, *5*, 567.
(73) Bavykin, D. V.; Friedrich, J. M.; Walsh, F. C. *Adv. Mater.* **2006**, *18*, 2807.
(74) (a) Armstrong, A. R.; Armstrong, G.; Canales, J.; Bruce, P. G. *Angew. Chem., Int. Ed.* **2004**, *43*, 2286. (b) Armstrong, G.; Armstrong, A. R.; Canales, J.; Bruce, P. G. *Chem. Commun.* **2005**, 2454. (c) Armstrong, A. R.; Armstrong, G.; Canales, J.; Bruce, P. G. *J. Power Sources* **2005**, *146*, 501.
(75) (a) Kavan, L.; Rathouský, J.; Grätzel, M.; Shklover, V.; Zukal, A. *J. Phys. Chem. B* **2000**, *104*, 12020. (b) Kavan, L.; Kalbac, M.; Zukalova, M.; Exnar, I.; Lorenzen, V.; Nesper, R; Grätzel, M. *Chem. Mater.* **2004**, *16*, 477. (c) Zukalová, M.; Kalbác, M.; Kavan, L.; Exnar, I.; Grätzel, M. *Chem. Mater.* **2005**, *17*, 1248.
(76) Reiman, K. H.; Brace, K. M.; Gordon-Smith, T. J.; Nandhakumar, I.; Attard, G. S.; Owen, J. R. *Electrochem. Commun.* **2006**, *8*, 517.
(77) Sugantha, M.; Ramakrishnan, P. A.; Hermann, A. M.; Warmsingh, C. P.; Ginley, D. S. *Int. J. Hydrogen Energy* **2003**, *28*, 597.
(78) Luo, J. Y.; Zhang, J. J.; Xia, Y. Y. *Chem. Mater.* **2006**, *18*, 5618.
(79) Jiao, F.; Bruce, P. G. *Adv. Mater.* **2007**, *19*, 657.
(80) (a) Wang, Y.; Cao, G. *Chem. Mater.* **2006**, *18*, 2787. (b) Wang, Y.; Takahashi, K.; Lee, K.; Cao, G. *Adv. Funct. Mater.* **2006**, *16*, 1133.
(81) (a) Spahr, M. E.; Bitterli, P.; Nesper, R.; Müller, M.; Krumeich, E.; Nissen, H. U. *Angew. Chem., Int. Ed.* **1998**, *37*, 1263. (b) Spahr, M. E.; Bitterli, P.; Nesper, R.; Haas, O.; Novák, P. *J. Electrochem. Soc.* **1999**, *146*, 2780.
(82) Patrissi, C. J.; Martin, C. R. *J. Electrochem. Soc.* **1999**, *146*, 3176.
(83) Lutta, S. T.; Dong, H.; Zavalij, P. Y.; Whittingham, M. S. *Mater. Res. Bull.* **2005**, *40*, 383.
(84) Sides, C. R.; Martin, C. R. *Adv. Mater.* **2005**, *17*, 125.
(85) (a) Takahashi, K.; Limmer, S. J.; Wang, Y.; Cao, G. *J. Phys. Chem. B* **2004**, *108*, 9795. (b) Takahashi, K.; Wang, Y.; Lee, K.; Cao, G. *Appl. Phys. A: Mater. Sci. Process.* **2006**, *82*, 27.
(86) Takahashi, K.; Wang, Y.; Cao, G. *J. Phys. Chem. B* **2005**, *109*, 48.
(87) Wang, Y.; Takahashi, K.; Shang, H.; Cao, G. *J. Phys. Chem. B* **2005**, *109*, 3085.
(88) Nordlinder, S.; Nyholm, L.; Gustafsson, T.; Edström, K. *Chem. Mater.* **2006**, *18*, 495.
(89) Long, J. W.; Dunn, B.; Rolison, D. R.; White, H. S. *Chem. Rev.* **2004**, *104*, 4463.
(90) Golodnitsky, D.; Nathan, M.; Yufit, V.; Strauss, E.; Freedman, K.; Burstein, L.; Gladkich, A.; Peled, E. *Solid State Ionics* **2006**, *177*, 2811.

CM702091Q